



Electrocoagulation associated with CO₂ mineralization applied to fluoride removal from mining industry wastewater

Elbert M. Nigri*, André L.A. Santos, Sônia D.F. Rocha*

Department of Mining Engineering, Universidade Federal de Minas Gerais, Av. Antônio Carlos, 6627, Bloco 2, Salas 4135/4414, Cep 31270-901, Belo Horizonte, Brazil, Tel. +55 31-3409-1931/1860; emails: elbertnigri@gmail.com (E.M. Nigri), sdrocha@demin.ufmg.br (S.D.F. Rocha), asantos@demin.ufmg.br (A.L.A. Santos)

Received 12 March 2020; Accepted 29 August 2020

ABSTRACT

Fluoride contamination causes serious environmental and health problems around the world. There are many alternatives to remove fluoride from wastewaters outstanding the electrocoagulation (EC) between them, although its application has been limited to a range of pH. The goal of this paper is the evaluation of diverse sources of CO₂ as a pH controller in order to work in the aluminum oxy-hydroxide stable zone. This improved the efficiency of fluoride removal from niobium processing wastewater allowing to comply with the target of the Brazilian regulation discharge limit of 10 mg L⁻¹. Batch and continuous EC experiments varying the electric current of 4.7 A (3.77 mA cm⁻²), 7.1 A (5.69 mA cm⁻²) and 9.4 A (7.53 mA cm⁻²), and gas flow rate (149, 186, and 248 mL min⁻¹) were carried out at an ambient temperature of 25°C. The fluoride residual concentration decreased from 134 to 1.4 mg L⁻¹ in the presence of CO₂, while the value of 36 mg L⁻¹ was observed in the absence of CO₂. The fluoride residual concentration of 8.1 mg L⁻¹, lower than the target of 10 mg L⁻¹ was obtained with the electric current of 9.4 A and the gas flow rate of 186 mL min⁻¹ (CO₂/N₂ 50%) while 11 mg L⁻¹ was obtained using the biogas containing 50.1% CO₂ and 47.9% CH₄. The dried sludge from EC is mainly composed of aluminum oxy-hydroxide and calcium carbonate, coherent with the capture and mineralization of CO₂ associated with the treatment of the effluent. The power consumption reached about 2.3 kWh m⁻³ and the electrode consumption varied in the range of 2.5–3.1 g L⁻¹.

Keywords: Electrocoagulation; Biogas; Aluminum hydroxide; Isotherm models; Fluoride adsorption

1. Introduction

Fluoride is an essential element for human health that in lower concentrations, between 0.4 and 1.0 mg L⁻¹, prevents dental diseases [1,2]. The World Health Organization (WHO) recommends the value of 1.5 mg L⁻¹ as the safe concentration of fluoride in water for human consumption [2]. Prolonged intake of water containing fluoride above 2 mg L⁻¹ may cause dental fluorosis and in extreme cases, serious diseases such as skeletal fluorosis, osteoporosis,

arthritis, male infertility, Alzheimer's disease, and liver, kidney or parathyroid lesions may occur [3–6].

Water contaminated by fluoride has been found naturally and serious environmental and health problems in several parts of the world have been occurred [5]. At least 25 countries around the world have been reported to be affected due to high fluoride concentrations in groundwater [7,8]. Moreover, fluoride contamination can result from the discharge to the environment of untreated industrial wastewaters from aluminum fluoride manufacturing,

* Corresponding authors.

semiconductors industries, fertilizer production, glass-manufacturing industries, and high strength and super-conducting metal alloys production [9,10].

Several methods have been used to reduce the fluoride content in water and thus making it suitable to discharge into the water bodies or even for human consumption [11]. Among those main methods, adsorption [12,13], chemical precipitation [14], ion exchange [15], reverse osmosis [16], electro dialysis [17], nanofiltration [18] and electrochemical processes [19] have been reported. Electrocoagulation effectiveness has been pointed out by several studies on the defluoridation of industrial wastewaters and water supplies [20–28].

Electrocoagulation is a technology that has experienced great popularity due to technical improvements. Also, it has played a prominent role in the treatment of drinking water as it exhibits some significant advantages such as a compact system associated with an automated and easy operation without chemical additives, high speeds of treatment and reduced amount of final sludge [29–33].

The coagulant species are formed *in-situ* as the sacrificial anode corrodes due to an electric current with simultaneous hydroxyl ions formation and the evolution of hydrogen gas at the cathode. These allow metallic hydroxides and hydroxyl complexes formation as well as the solids removal by flotation. Iron and aluminum are the most used metals as cathodes and hydroxide flocs formed can also act as adsorbents for ions [33]. Emamjomeh et al. [34] proposed that the mechanism of the fluoride removal by electrocoagulation is not only the adsorption of F^- but also the possible formation of solid cryolite (Na_3AlF_6) in the final pH range of 5–8 in the reactor. Besides, these authors state that the defluoridation process is more efficient at the final pH from 6 to 8.

Ezzeddine et al. [35] reported higher fluoride removal in pH below 7, which was correlated to the formation of gibbsite ($Al(OH)_3$) that presents low solubility and therefore higher stability. On the other hand, the formation of aluminum fluorohydroxide complex has been reported as the main reason for defluoridation effectiveness by electrocoagulation [34,36–40]. Another factor that contributes to fluoride removal is the diminished concentration of OH^- ions at lower pH (5.5–7.5) if compared to hydroxyl ions in alkaline solution. Likewise, the presence of OH^- ions changes the formation of AlF_6^{3-} species that are required to the cryolite formation [20,34,36].

Usually pH increases during electrocoagulation (EC) depending on the feed pH. If the pH rises above 8, the gibbsite formation is unfavorable due to its greater stability in the pH 6–8 range [20,24,34,38,41–43]. Instead of HCl or H_2SO_4 as pH controllers, the use of CO_2 does not disturb the chloride and sulfate concentrations in the aqueous treated stream, thus contributing to the reduction of greenhouse gas emission. Specifically, the use of CO_2 generated by a biodigester works as a separation process of methane from the gas, which favors its use for power generation.

Taking into consideration the aspects presented, the purpose of this study is the evaluation of fluoride removal from a real effluent by the electrocoagulation process using distinct sources of CO_2 as a process pH regulator. Batch and continuous electrocoagulation experiments integrated in

a pilot biodigester and wastewater electrocoagulation unit were performed to assessing the efficacy of the process.

2. Materials and methods

2.1. Experimental setup

The experiments were carried out in an acrylic reactor with a depth of 18 cm, with of 15 cm and length of 20 cm, and a useful volume of submerged plates of 3.72 L applying 8 aluminum plates of 20 cm height, 13 cm wide and 2 mm thickness, with the distance inter-electrodes of 0.5 cm as depicted in Fig. 1. The submerged height of each plate was 12 cm, becoming an immersed area per plate of 312 cm². The mixture in the system was carried out by a magnetic stirrer. The aluminum plates were previously immersed in a 0.1 mol HCl solution for 10 min, washed in water, dried, and their mass was measured in each experiment.

The EC was performed by galvanostatic mode with a fixed electric current of 9.4 A with electrodes connected in a monopolar configuration. Samples of 20 mL were taken out, filtered through a paper filter with 2 μm porosity and stored in plastic bottles for chemical analysis. All experiments were carried out for 60 min in triplicate.

The gas injection system was composed of a CO_2 cylinder (13.5 L) and an N_2 cylinder (50 L) or a biodigester HomeBiogas (Israel) of 1,200 L of digestion volume and a gas tank of 700 L. Both of them were set up with a flow control Flowmeter 2510A2A15BNBN, 1–10 LPM Air. The biodigester gas is composed of 50.1% CO_2 , 47.9% CH_4 , 0.8% O_2 , 40 ppm (CO), and 7 ppm (H_2S) indicated by the gas analyzer Landtec G5000 (EUA) that was used to characterize the gas generated by the biodigester.

2.1.1. Batch electrocoagulation experiments

Batch tests were performed in the system setup shown in Fig. 1a in different conditions as described below:

- Without pH control neither injection of gas in the effluent;
- The pH was set at 6.3 adding HNO_3 (PA ACS) in the effluent;
- The pH of effluent was decreased with the injection of pure CO_2 until the pH stabilized at 6.3. After that, the DC power supply was turned on and the gas flow was regulated to keep the pH at 6.3.
- The pH of effluent was decreased with the injection of a mixture of CO_2 (50%) and N_2 (50%) using the same procedure described in section 2.1.1. The proportion of CO_2 in the gas mixture was chosen to simulate the CO_2 concentration of the biogas.
- The pH was decreased and kept at pH 6.3 with biogas injection by the same procedure described in section 2.1.1.

2.1.2. Continuous experiments

Continuous tests were carried out in the same experimental setup in two distinct conditions: (i) with a gas mixture containing CO_2 – 50% and N_2 – 50% and (ii) with the biodigester's gas. The effluent was pumped simultaneously to the gas, flowing them through the mixer (Fig. 1b L) and feeding

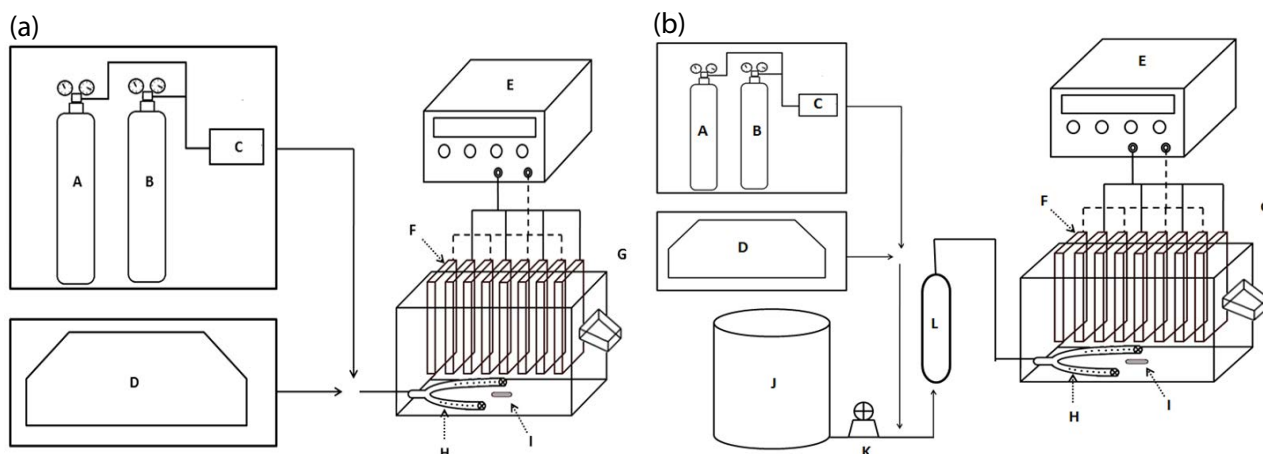


Fig. 1. Experimental setup: (a) batch process and (b) continuous process. (A) CO₂ cylinder; (B) N₂ cylinder; (C) gas mixer; (D) biogas digester; (E) DC power supply; (F) aluminum electrodes; (G) electrochemical cell; (H) gas/wastewater sprinkler; (I) magnetic stirrer; (J) wastewater storage; (K) peristaltic pump; (L) gas and wastewater mixer.

to the electrochemical cell (Fig. 1b G) through the gas/wastewater sprinkler (Fig. 1b H).

This procedure was carried out until the electrochemical cell was completely filled. Then the effluent flow was temporarily interrupted turning off the peristaltic pump (Fig. 1b K) until the pH reached the set point pH 6.3 once the injection of gas was maintained. Thereafter, the DC power supply was switched on and after one residence time, the effluent pump was re-started. This procedure aimed at the initial stabilization of the continuous system.

When the experiments were performed with CO₂/N₂ mixture, the effluent flow rate was varied in 248, 186 and 148.8 mL min⁻¹ corresponding to the residence times of 25, 20 and 15 min, respectively, and changing the current in 9.4, 7.1 and 4.7 A (current densities of 7.53, 5.69 and 3.77 mA cm⁻²), respectively. Experiments were carried out also using biogas, with a current of 9.4 A (7.53 mA cm⁻²) and a flow rate of 186 mL min⁻¹. In the present study, the usual kinetic and thermodynamic evaluation were used to obtain the process isotherms.

2.2. Wastewater samples

Samples of wastewater were provided from the Niobium Processing Wastewater Industry and stored at room

temperature 25°C ± 5°C in a container of 1,000 L. Chemical analysis has been periodically carried out in order to verify its stability.

2.3. Solids and solutions characterization

Table 1 presents the parameters and the respective analytical methods from Standard Methods for the Examination of Water and Wastewater used for aqueous solutions characterization. The solids of electrocoagulation were characterized regarding their functional groups, by Fourier-transform infrared spectroscopy (FTIR) (Bruker Alpha, EUA), attenuated total reflectance, diffuse reflectance accessory; chemical elements, by X-ray fluorescence (XRF) (PANalytical PW2400, UK); crystalline phase identification, by X-ray diffractometer. Optical images were obtained with a microscope model NOVEL BM2100POL model with an image capture camera.

2.4. Modeling parameters

The current density was determined by Eq. (1), while the energy consumption was calculated by Eq. (2).

$$\delta = \frac{i}{A} \quad (1)$$

Table 1
Methods of analysis used to characterize the wastewater [44]

Parameters	Analysis method
Fluoride	Specific ion electrode Thermo Scientific Orion 9609BNWP (EUA) in TISAB IV solution prepared by dissolving tris(hydroxymethyl)aminomethane and sodium tartrate in HCl and water
Ca, Na, Mg, Al	GBC atomic absorption spectrophotometer, Model AVANTA
Alkalinity, chlorides	Titimetry
COD	Closed reflux colorimetric method for low COD range
Sulfate	Turbidimetry
pH, conductivity	Instrumental
Total phosphorus	Colorimetric

where δ is the current density (mA cm^{-2}), i is the current (mA) and A is the submerged area of the electrode (anode, cm^2), E_c is the energy consumption (Wh), U is the electric tension (V), t is time (h) and V is the treated effluent volume (L).

$$E_c = \frac{U \cdot i \cdot t}{V} \tag{2}$$

The amount of metal consumed in the plates depends on the amount of electricity passing through the electrocoagulation cell and the residence time of treatment and it can be calculated by Faraday’s law represented in Eq. (3) [45–47].

$$m = \varphi \frac{i \cdot t \cdot W}{n \cdot F} \tag{3}$$

where m is the mass of the electrode consumed (g), i is the current density (mA cm^{-2}), t is time (s), W is the molar mass of the electrode material (g mol^{-1}), n is the number of electrons in the redox reaction and F is the Faraday constant ($96,485 \text{ C mol}^{-1}$). When parallel reactions occur, the correction factor denoted current efficiency or faradic yield (φ) must be used to consider the difference between the theoretical and experimental dissolution of the sacrificial anode [38,48–50].

Considering the contribution of adsorption in electrocoagulation, isotherm models have been used in literature to correlate the amount of contaminants removed with the amount of solids formed. Differently from conventional adsorption tests in which it is possible to fix the amount of adsorbent, this is not possible in the electrocoagulation batch tests. In order to evaluate the kinetic models of the reaction, first-order and second-order equations were used (Table 2). The removal of fluorides by electrocoagulation does not involve only the phenomenon of adsorption. Phenomena such as ion exchange and precipitation are also observed [34]. However, the phenomena of precipitation and ion exchange do not limit the application of kinetic and isothermal models [45–47,51,52]. This fact can be seen in the use of bone char as an adsorbent in the removal of fluorides in which phenomena such as adsorption, ion exchange, and precipitation have been observed [12,53]. The Freundlich, Langmuir, Redlich–Peterson, Sips, and Temkin isotherm models (Table 3), in their general form, were used to evaluate the results in this work.

The OriginPro8 software was used to obtain the parameters’ models of data fitting. The evaluation of the quality of curves adjustment was done by the nonlinear chi-square test (χ^2) (Eq. (4)). Lower values of χ^2 indicate similarities between predicted and experimental data while

larger values represent their distance. In Eq. (4), θ is C_t for kinetic models and q_e for isotherms models.

$$\chi^2 = \sum_{i=1}^n \frac{(\theta_{\text{calc}} - \theta_{\text{meas}})^2}{\theta_{\text{meas}}} \tag{4}$$

3. Results and discussion

3.1. Wastewater characterization

Table 4 presents the parameters of the wastewater from the Niobium Processing Mineral Industry (Brazil) used in this study. Presenting a high concentration of chloride and sodium of 1,424 and 632 mg L^{-1} , respectively, the effluent also presents organic compounds derived from flotation ore that was measured as chemical oxygen demand (COD) of 106 $\text{mgO}_2 \text{ L}^{-1}$, and significant fluoride content of (134 mg L^{-1})

Table 3
Isotherm equations of Freundlich, Langmuir, Redlich–Peterson, Sips and Temkin adsorption models

Model	Equation	References
Freundlich	$q_e = K_f C_e^{1/n}$	[54]
Langmuir	$q_e = \frac{q_m K_L C_e}{1 + K_L C_e}$	[55]
Redlich–Peterson	$q_e = \frac{K_{RP} C_e}{1 + a_{RP} C_e^b}$	[56]
Sips	$q_e = \frac{q_{ms} K_s C_e^{ms}}{1 + K_s C_e^{ms}}$	[57]
Temkin	$q_e = \frac{RT}{b} \ln(K_t C_e)$	[58]

Table 4
Chemical characterization of Brazilian mineral industry wastewater

Parameter	Value
pH	7.8
Conductivity ($\mu\text{S cm}^{-1}$)	6,056.0
Fluoride (mg L^{-1})	134.0
Calcium (mg L^{-1})	4.4
Sodium (mg L^{-1})	632.0
Aluminum (mg L^{-1})	<5.0
Chloride (mg L^{-1})	1,424.0
Sulfate (mg L^{-1})	69.0
Alkalinity carbonates and hydroxides (mg L^{-1})	0.0
Alkalinity bicarbonates (mg L^{-1})	660.0
Total phosphorus (mg L^{-1})	8.0
COD ($\text{mgO}_2 \text{ L}^{-1}$)	106.0

Table 2
Kinetic models applied in electrocoagulation tests

Models	Equation	References
Pseudo-first-order	$C_t = C_0 e^{-k_1 t}$	[45,46]
Pseudo-second-order	$\frac{1}{C_t} = \frac{1}{C_0} + k_2 t$	

that to be removed. This effluent does not comply with the Brazilian guideline of 10 mg L^{-1} of fluorides to be released into a water body and requires proper treatment [59].

3.2. Batch experiments

Fig. 2 shows the variation of fluoride concentration and pH with electrocoagulation time for tests in the following conditions (i) without pH control, (ii) pH control with HNO_3 , (iii) pH adjustment with CO_2 , (iv) CO_2/N_2 50%, and (v) biogas injection.

The use of HNO_3 , CO_2 , CO_2/N_2 50%, and biogas in pH adjustment has presented the same behavior for fluoride removal. Although the use of biogas had shown a slightly over residual fluoride concentration, in all cases with pH control the residual fluoride concentrations were lower than the Brazilian standard wastewater discharge (10 mg L^{-1}) [59]. Moreover, it was possible to obtain fluoride residual concentration below the limit of 1.5 mg L^{-1} established by the World Health Organization (WHO, 1998) for HNO_3 (1.0 mg L^{-1}) and CO_2 (1.4 mg L^{-1}) after 60 min. In addition, the fluoride residual concentrations of CO_2/N_2 50% and biogas were very low, 1.9 and 4.0 mg L^{-1} , respectively.

The final pH must be between pH 6 and 9 in order to direct discharge into the watercourse. To keep the pH around 6–9 the gas flow applied was 1.75, 1.80, and 1.25 L min^{-1} for the CO_2 , CO_2/N_2 50%, and biogas, respectively. Additionally, the nitric acid consumption has shown an average value of $3.23 \text{ mL L}_{\text{effluent}}^{-1}$ of HNO_3 PA.

Final pH values of 6.60, 6.50, 6.60, and 8.10 for HNO_3 , CO_2 , CO_2/N_2 50%, and biogas were observed at the end of the EC tests respectively (Table 5). The use of HNO_3 , CO_2 , CO_2/N_2 50% indicated the possibility to maintain the pH within the range of lower solubility for aluminum hydroxide, the main specie responsible for the coagulation effect. The observed increase in the final pH to 8.10 in EC with biogas was due to an eventual drop in biodigester pressure that caused one reduction in the biogas flow rate.

In EC tests were the pH was not controlled with gas either with nitric acid, the removal of fluoride has been 75% with the fluoride residual concentration of 36 mg L^{-1} and final pH 10.3. This condition was not adequate to treat the effluent to the required standards. The final aluminum concentration was below 5 mg L^{-1} , the limit of detection of analytical technique, when HNO_3 , CO_2 , CO_2/N_2 50%, and biogas were used while the residual aluminum concentration was 23 mg L^{-1} without acid addition. These results corroborate the fact that the pH close to 6.3 provides greater stability to $\text{Al}(\text{OH})_3$ species that is mainly responsible for removing fluoride by adsorption [37,60].

Table 5 shows the consumption of energy and electrodes for the EC tests of fluoride removal with none addition, adding HNO_3 and injecting CO_2 , CO_2/N_2 50%, or biogas.

The average power and the aluminum electrodes consumption were 7.0 kWh m^{-3} and 2.2 g m^{-3} . However, the residual fluoride concentration of 10 mg L^{-1} was reached at a shorter time, which could reduce the treatment time to 20 min instead of 60 min. This fact considerably reduces the power and electrodes consumption to 2.35 kWh m^{-3} and 0.73 g m^{-3} .

Pseudo-first and second-order models were used to evaluate the kinetic data (Fig. 3 and Table 6) for the electrocoagulation in the presence of biogas. Both models presented good fitting with similar correlation coefficients (R^2) equal to 0.9897 (pseudo-first-order) and 0.9841 (pseudo-second-order). However, the pseudo-first-order model presents a higher deviation than the pseudo-second-order model, indicated by the χ^2 value.

Fig. 4 shows the data fitting of the Langmuir, Freundlich, Redlich–Peterson, Sips, and Temkin isotherms models on the fluoride removal by electrocoagulation with the biogas injection in a batch process. The parameters obtained from these data fitting are shown in Table 7. Sips' isotherm presents the best data fit ($R^2 = 0.9806$) followed by the Temkin's isotherm with a correlation coefficient of 0.9621.

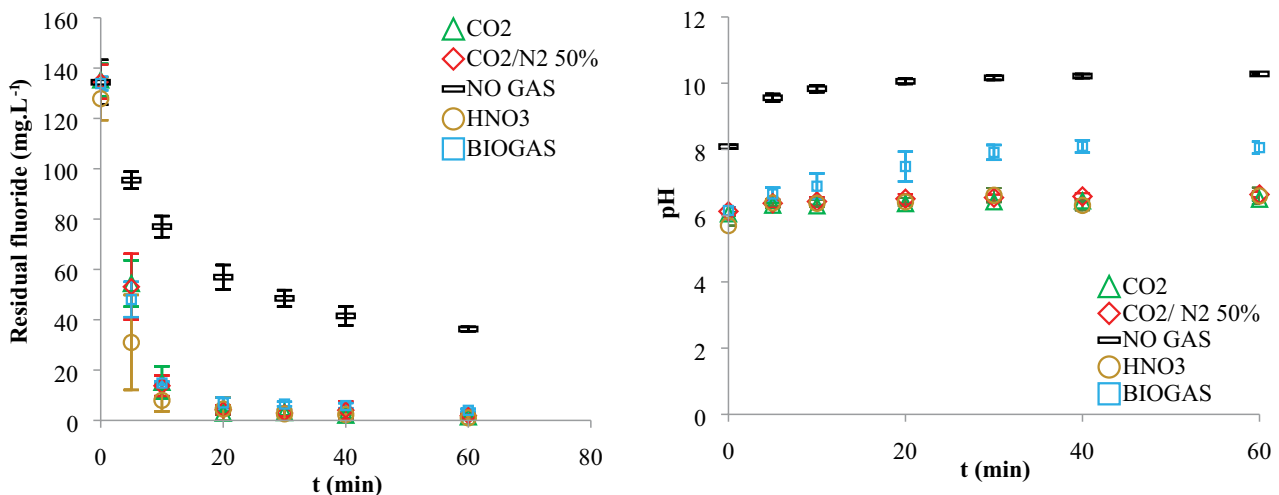


Fig. 2. Evolution of residual fluoride concentration in the electrocoagulation batch process. Monopolar configuration; electrodes number 8; electric current 9.4 A; submerged area 312 cm^2 per plate; electric current density 7.53 mA cm^{-2} ; initial temperature $25^\circ\text{C} \pm 2^\circ\text{C}$; treated volume 3.72 L .

Table 5
Consumption of energy and electrodes on batch tests

Experiment	Biogas	CO ₂	CO ₂ /N ₂ 50%	HNO ₃	No gas
Current density (mA cm ⁻²)	7.53	7.53	7.53	7.53	7.53
Current (A)	9.40	9.40	9.40	9.40	9.40
Tension (V)	2.77	2.90	2.77	2.60	2.85
Power consumption (kWh m ⁻³)	6.99	7.33	6.99	6.57	7.20
Electrodes consumption (g L ⁻¹)	2.11	1.60	1.90	2.46	2.39
Residual fluoride (mg L ⁻¹)	4.00	1.40	1.90	1.00	36.30
pH final	8.10	6.50	6.60	6.60	10.30

Monopolar configuration; electrodes number 8; electric current 9.4 A; submerged area 312 cm² per plate; electric current density 7.53 mA cm⁻²; initial temperature 25°C ± 2°C; treated volume 3.72 L; experimental time 60 min.

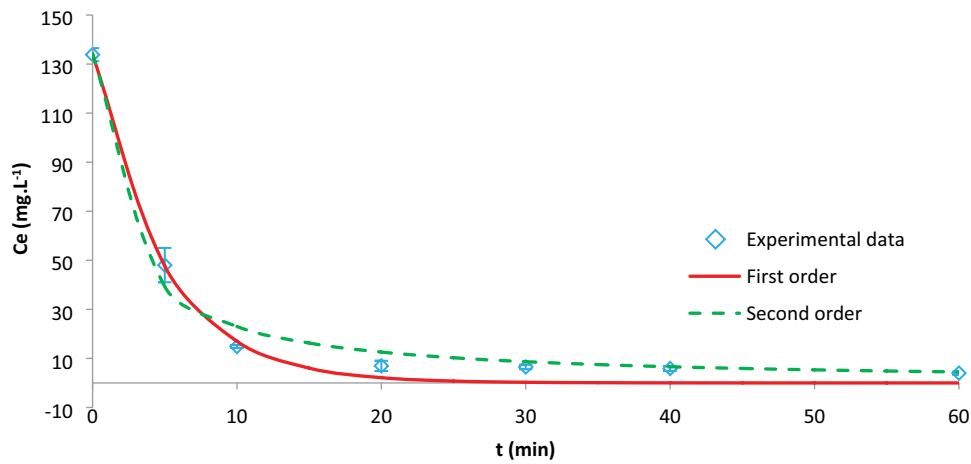


Fig. 3. Kinetic models of fluoride removal by electrocoagulation batch process in the presence of biogas. Monopolar configuration; electrodes number 8; electric current 9.4 A; submerged area 312 cm² per plate; electric current density 7.53 mA cm⁻²; initial temperature 25°C ± 2°C; treated volume 3.72 L.

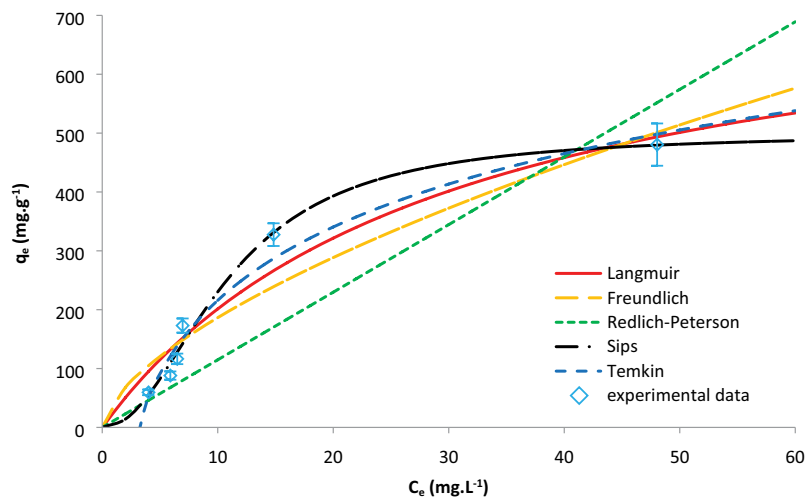


Fig. 4. Langmuir, Freundlich, Redlich–Peterson, Sips, and Temkin isotherms data fitting on fluoride removal by electrocoagulation batch process in the presence of biogas. Monopolar configuration; electrodes number 8; electric current 9.4 A; submerged area 312 cm² per plate; electric current density 7.53 mA cm⁻²; initial temperature 25°C ± 2°C; treated volume 3.72 L; experimental time 60 min; φ = 2.5.

Table 6

Parameters of data fitting of pseudo-first and pseudo-second-order kinetic models for fluoride removal by electrocoagulation in batch mode using biogas

Batch process							
Pseudo-first-order				Pseudo-second-order			
k_1 (min ⁻¹)		R^2_{Adj}	χ^2	k_2 (mg ⁻¹ min ⁻¹)		R^2_{Adj}	χ^2
Value	Error	Value	Value	Value	Error	Value	Value
0.2066	0.0175	0.9897	19.4267	0.0036	5.8515e ⁻⁴	0.9841	11.5130

Monopolar configuration; electrodes number 8; electric current of 9.4 A; submerged area of 312 cm² per plate; electric current density: 7.53 mA cm⁻²; initial temperature: 25°C ± 2°C; treated volume: 3.72 L; experimental time: 60 min.

Table 7

Parameters of Langmuir, Freundlich, Redlich–Peterson, Sips, and Temkin isotherms data fitting on fluoride removal by electrocoagulation batch process in the presence of biogas

Langmuir	q_m (mg g ⁻¹)	K_L (L mg ⁻¹)		R^2_{Adj}	χ^2
	798.2661	0.0337		0.9226	60.0942
Freundlich	K_F (mg g ⁻¹)(L mg ⁻¹) ^{1/n}	n		R^2_{Adj}	χ^2
	43.7260	1.5877		0.8733	91.9054
Temkin	K_T (L mg ⁻¹)	b		R^2_{Adj}	χ^2
	0.3321	0.0056		0.9621	5.4112
Redlich–Peterson	K_{RP} (L g ⁻¹)	a_{RP}	β	R^2_{Adj}	χ^2
	11.4856	1.0939	-7.8978e ⁷	0.4950	25.9579
Sips	q_{ms} (mg g ⁻¹)	K_S (L mg ⁻¹) ^{ms}	ms	R^2_{Adj}	χ^2
	500.2213	0.0067	2.1055	0.9806	12.1576

Monopolar configuration; electrodes number 8; electric current 9.4 A; submerged area 312 cm² per plate; electric current density 7.53 mA cm⁻²; initial temperature 25°C ± 2°C; treated volume 3.72 L; experimental time 60 min; $\varphi = 2.5$.

Sips' isotherm equation derives from the limiting behavior of Langmuir and Freundlich isotherms [61] and is characterized by the inclusion of the dimensionless heterogeneity factor (ms). When ms is equal to 1, the Sips equation is converted to the Langmuir isotherm equation, implying a homogeneity in the adsorption. For the present system, the ms value of 2.1055 means that there are interactions between the adsorption sites.

It was also possible to observe that the experimental data is better fitted by the Langmuir isotherm model, with an R^2 value of 0.9226, compared to 0.8733 for the Freundlich isotherm model, thus suggesting that the adsorption cannot be characterized as totally homogeneous neither tally heterogeneous. The b parameter = 0.0056 from Temkin's isotherm, greater than zero indicates an adsorption process slightly endothermic.

3.3. Continuous electrocoagulation experiments

Continuous experiments were carried out with the CO₂/N₂ 50% gas mixture and also with biogas injection. Fig. 5 shows the residual fluoride concentration obtained at the output of the continuous system using currents of 4.7 A (3.77 mA cm⁻²), 7.1 A (5.69 mA cm⁻²), and 9.4 A (7.53 mA cm⁻²).

The continuous process reduced the inlet fluoride concentration of 136.0 mg L⁻¹ to 7.9, 13.2, and 30.7 mg L⁻¹ by using an electric current density of 7.53, 5.69, and 3.77 mA cm⁻², respectively. For these tests, the wastewater flow rate

186 mL min⁻¹ and the gas mixture CO₂/N₂ 50% were utilized. These results suggest that an increase in density current improved fluoride removal.

The wastewater flow rate was also varied (Fig. 6) and average residual fluoride concentrations at the output of the continuous system were 14.4, 7.9, and 5.6 mg L⁻¹ for 248 to 186 and 149 mL min⁻¹, respectively, were obtained.

Table 8 summarizes the power and electrodes consumption for continuous tests. As the objective of this treatment is to reduce the fluoride concentration below 10 mg L⁻¹, the current of 9.4 A, and flow rate of 186 mL min⁻¹ were chosen for continuous experiments with the biogas injection that allowed to reach a fluoride concentration of 10.3 mg L⁻¹ and pH 7.1 (Figs. 5, 6 and Table 8). The results demonstrate that electrocoagulation was technically efficient to fluoride removal and CO₂ in distinct mixtures could be used as a pH controller in the system.

In general, increasing the electrode and power consumption for continuous experiments has been observed. The energy consumption of 2.25 kWh m⁻³ and electrode consumption of 2.52 g L⁻¹ were obtained using an electric current of 9.4 A (7.53 mA cm⁻²) and a flow rate of 186 mL min⁻¹ of the gas CO₂/N₂ 50%. The values observed when biogas was used were slightly higher, 2.36 kWh m⁻³ and 3.09 g L⁻¹, respectively.

These results obtained in the present work contribute to support the integration of water/wastewater treatment with biogas production systems for many purposes.

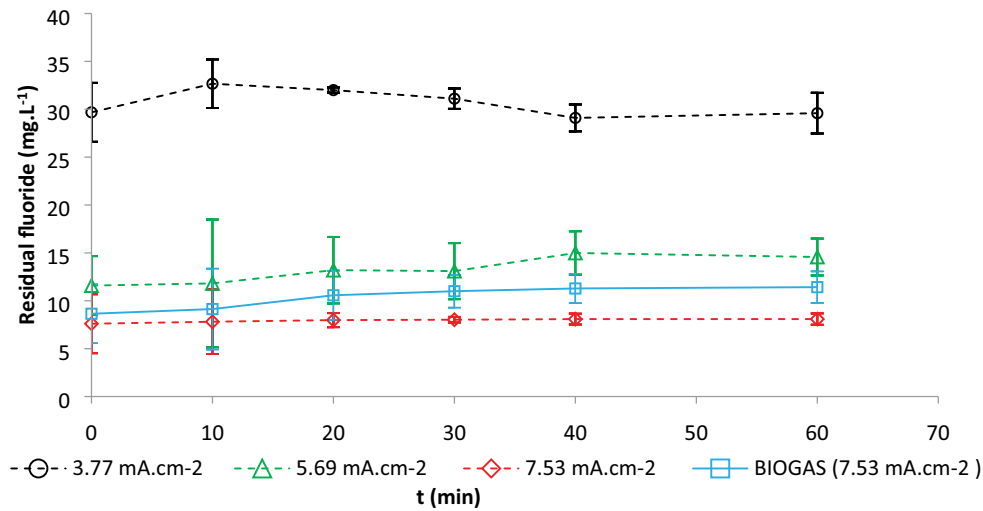


Fig. 5. Continuous tests for fluoride removal with electric currents of 4.7 A (3.77 mA cm^{-2}), 7.1 A (5.69 mA cm^{-2}) and 9.4 A (7.53 mA cm^{-2}) using CO_2/N_2 50% and biogas test 9.4 A (7.53 mA cm^{-2}). Flow rate 186 mL min^{-1} ; monopolar configuration; electrodes number 8; submerged area 312 cm^2 per plate; electrochemical cell volume 3.72 L; initial temperature $25^\circ\text{C} \pm 2^\circ\text{C}$; residence time 20 min; initial fluoride concentration 134 mg L^{-1} .

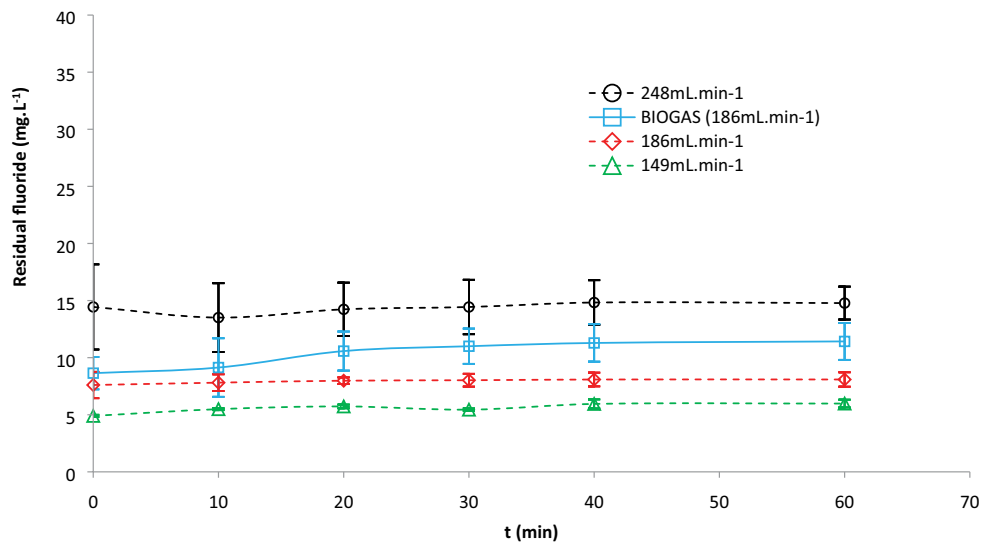


Fig. 6. Continuous tests for fluoride removal with flow rate variation in 149, 186 and 248 mL min^{-1} using CO_2/N_2 50% and biogas (186 mL min^{-1}). Current of 9.4 A (7.53 mA cm^{-2}); monopolar configuration; electrodes number 08; submerged area 312 cm^2 per plate; electrochemical cell volume 3.72 L; initial temperature $25^\circ\text{C} \pm 2^\circ\text{C}$; initial fluoride concentration 134 mg L^{-1} .

The electrocoagulation acts also as a separation process of CO_2 from CH_4 contained in the biogas which is an additional advantage of this system. As a result, the gas effluent from the electrocoagulation system is composed mainly of residual CO_2 , methane (from biogas), H_2 (from EC process), and other minor gases generated by the decomposition of the biomass.

3.4. Residual solid characterization

Fig. 7 shows the morphology of residual solids from tests with biogas and CO_2 injection. Grains in the form of brittle crystals of varying sizes may be identified.

Fig. 8 shows FTIR analysis of residual solid by EC tests: without gas injection, inserting HNO_3 , injecting CO_2 , injecting CO_2/N_2 50% and injecting biogas. The results are very similar, except for the test sample without gas injection, which shows more prominent bands in the FTIR due to greater crystallinity of the solids which agrees with it has been well-defined peaks in the diffraction pattern. The bands of $3,545$; $3,466$ and $3,420 \text{ cm}^{-1}$ represent the H–O–H stretch [19,28,41,62] and the band $3,696$ and $1,640 \text{ cm}^{-1}$ represents the hydroxyl and water (OH) flexion [19,63,64].

The peaks 438 and 465 cm^{-1} indicate the presence of sulfates and the peak 872 cm^{-1} indicates the presence of phosphate [65]. The peak $1,081 \text{ cm}^{-1}$ indicates the symmetrical

Table 8

Power and electrode consumption in continuous electrocoagulation experiments of fluoride removal with a gas mixture of CO₂/N₂ 50% and biogas as pH controllers

Experiment	149 mL min ⁻¹	186 mL min ⁻¹	248 mL min ⁻¹	4.7 A	7.1 A	9.4 A	Biogas
Current density (mA cm ⁻²)	7.53	7.53	7.53	3.77	5.69	7.53	7.53
Current (A)	9.40	9.40	9.40	4.70	7.10	9.40	9.40
Tension (V)	2.70	2.67	2.83	2.30	2.40	2.67	2.80
Cons. power (kWh m ⁻³)	2.84	2.25	1.79	0.97	1.53	2.25	2.36
Electrodes consumption (g L ⁻¹)	2.45	2.52	2.28	1.14	2.13	2.52	3.09
Flow rate (mL min ⁻¹)	149.00	186.00	248.00	186.00	186.00	186.00	186.00
Residual fluoride (average) (mg L ⁻¹)	5.60	7.90	14.40	30.70	13.20	7.90	10.30
pH (average)	6.40	6.50	6.50	6.70	6.50	6.50	7.10

Monopolar configuration; electrodes number 8; submerged area 312 cm² per plate; initial temperature 25°C ± 2°C; initial fluoride concentration 134 mg L⁻¹.

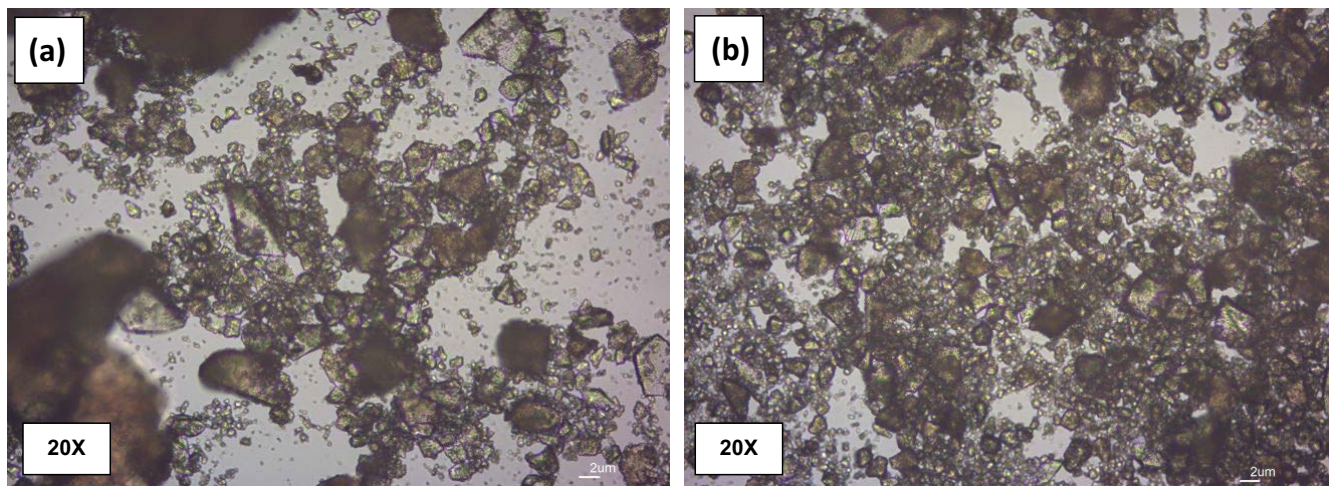


Fig. 7. Optical microscope images of residual solid of batch electrocoagulation experiments applying biogas (a) CO₂ and (b) injection as pH controllers.

stretch and 1,400 cm⁻¹ the asymmetric stretch of CO, and peaks 872 and 713 cm⁻¹ due to the presence of CO₃²⁻ [66,67] which indicate the CO₂ mineralization.

It is also possible to view bands associated with aluminum connections at 1,382 cm⁻¹ with the stretching in Al–H [19], at 1,060 cm⁻¹ the stretching of Al–O [41] is observed, and the flexion of Al–OH is represented by the band at 990 cm⁻¹ [19]. The flexion Al–F–Al is represented by the band at 630 cm⁻¹ [28,68] and the band at 585 cm⁻¹ can be attributed to the stretching of Al–OH [19].

The phase and chemical characterization of the solids formed are very similar, independent of the experimental condition. Chemical analysis of residual solids from EC tests has pointed out Al, Na, Cl, O, and F, as main elements, and Si, S, Ca, Fe, K, Cr as traces. The pattern of DRX (Fig. 9) exhibits mainly aluminum oxide hydroxide as a crystalline phase (AlO(OH), Al(OH)₃, Al(OH,F)₃). However, the residual solid from the test without gas injection exhibits better crystallinity than the residual solids from those tests with injection or addition of external species (HNO₃, CO₂, CO₂/N₂ 50%, and biogas).

The residual solids present a certain degree of amorphous solids which difficult the phase characterization mainly derived from the superposition of peaks. In addition, the content of calcium and the competition of fluoride and carbonate for calcium ions could contribute to the low quantity and imposes difficulties on carbonate phases identification. Nevertheless, the carbonate phases were found and their presence was corroborated due to the C–O and CO₃ bands identified by the FTIR spectra analysis.

It was possible to observe the presence of carbonates either in solids obtained from tests without gas addition, only with HNO₃, due to the initial bicarbonate alkalinity of wastewater. However, in the presence of CO₂, the presence of calcium carbonate polymorphs was more pronounced. These are evidence of CO₂ mineralization that could be better observed at higher calcium concentrations when the competition between fluoride and carbonate to calcium ions would be not significant. At this stage, it was not possible to quantify the degree of mineralization of CO₂, and this must be taken into account in future studies.

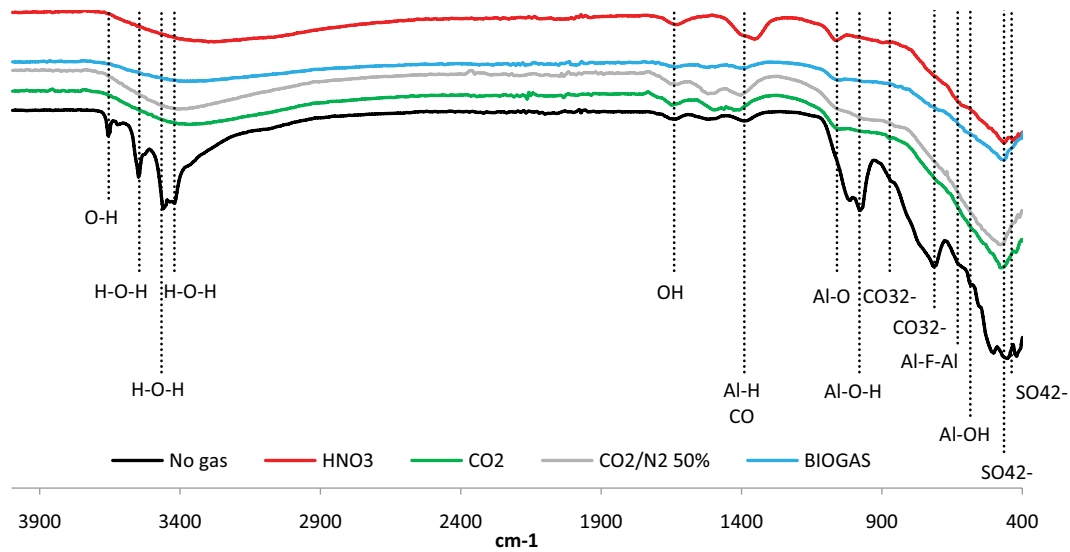


Fig. 8. FTIR spectra for residual solid from electrocoagulation experiments without gas addition, and with HNO_3 , CO_2 , CO_2/N_2 50%, and biogas injection.

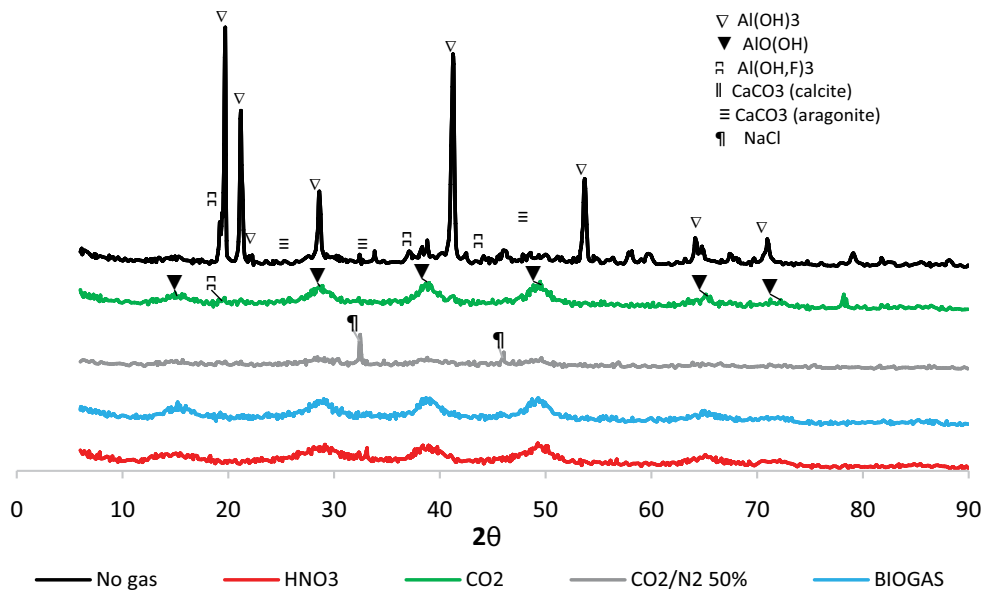


Fig. 9. X-ray diffractograms for residual solid from electrocoagulation experiments without gas addition, and with HNO_3 , CO_2 , CO_2/N_2 50%, and biogas injection.

The fluoride content in all the residual solids is quite similar. Furthermore, the use of biogas or any other source of gas containing CO_2 can be adequate to keep the pH of the solution in the pH range of lower solubility of aluminum hydroxide, thus contributing to the higher efficiency of electrocoagulation.

4. Conclusion

The use of CO_2 as a pH controller agent in the electrocoagulation system resulted in a reduction of residual fluoride concentration up to 1.4 mg L^{-1} compared to the

system without CO_2 use (36 mg L^{-1}). The results demonstrate that the fluoride removal process was also efficient applying biogas (50.1% CO_2 , 47.9% CH_4 , 0.8% O_2 , 40 ppm CO and 7 ppm H_2S) as a pH regulator of the system and an additional benefit of the process is the CO_2 capture and storage by mineralization.

The electrodes and power consumption may be raised due to the increment of electric current from 4.7 (3.77 mA cm^{-2}) to 9.4 A (7.53 mA cm^{-2}) and also due to the decrease of gas flow rate from 286 to 149 mL min^{-1} . The experiment applying an electric current 9.4 A, CO_2/N_2 50% gas flow rate of 186 mL min^{-1} showed a power and aluminum consumption

of 2.25 kWh m⁻³ and 2.52 g L⁻¹, respectively, to produce a treated effluent containing a fluoride residual concentration of 8.1 mg L⁻¹. The use of biogas in the same conditions makes the power and electrodes consumption slightly higher in 2.36 kWh m⁻³ and 3.09 g L⁻¹ producing a treated effluent with fluoride residual concentration of 11 mg L⁻¹.

According to the characterization of the solids, the solids are made up mostly of hydroxides and aluminum oxides. The presence of fluoride and carbonates was also observed, which may be an indication of CO₂ mineralization associated with the fluoride removal.

Symbols

A	— Submerged area of the electrode, cm ²
a_{RP}	— Redlich–Peterson constant
b	— Temkin constant
C_e	— Concentration at equilibrium time, mg L ⁻¹
C_0	— Initial concentration, mg L ⁻¹
C_t	— Concentration at time t , mg L ⁻¹
EC	— Electrocoagulation
E_c	— Energy/power consumption, Wh
F	— Faraday constant, C mol ⁻¹
i	— Electric current, A
k_1	— Pseudo-first-order constant, s ⁻¹
k_2	— Pseudo-second-order constant, s ⁻¹
K_F	— Freundlich isotherm constant, (mg g ⁻¹)(L mg ⁻¹) ^{1/n}
K_L	— Constant related to the energy of adsorption, mg L ⁻¹
K_{RP}	— Redlich–Peterson adsorption constant, L g ⁻¹
K_S	— Sips adsorption constant, (L mg ⁻¹) ^{ms}
K_T	— Temkin adsorption constant, mg g ⁻¹
m	— Mass of electrode consumed, g
ms	— Dimensionless heterogeneity factor
n	— Number of electrons in the redox reaction
n	— Freundlich constant
q_e	— Adsorption capacity, mg g ⁻¹
q_m	— Langmuir adsorption capacity, mg g ⁻¹
q_{ms}	— Sips Adsorption capacity, mg g ⁻¹
R	— Ideal gas constant, 8.314 J(K mol) ⁻¹
t	— Time, h, min, s
U	— Electric tension, V
V	— Volume of treated effluent, L
W	— Molar mass of electrode material, g.mol ⁻¹
T	— Temperature absolute, K
δ	— Current density, mA cm ⁻²
φ	— Current efficiency/faradic yield
β	— Redlich–Peterson constant
x^2	— Error
θ_{calc}	— Calculated data
θ_{meas}	— Measured data

Acknowledgment

The authors acknowledge the financial support from the Brazilian Research funding agencies CAPES for the post-doctoral scholarship, CNPq (Process 308044/2018-5) and FAPEMIG.

References

- [1] S. Ghorai, K.K. Pant, Investigations on the column performance of fluoride adsorption by activated alumina in a fixed-bed, *Chem. Eng. J.*, 98 (2004) 165–173.

- [2] WHO, Guidelines for Drinking Water Quality, 2nd ed., Addendum to Health Criteria and Other Supporting Information, Vol. 2, World Health Organization, Geneva, 1998, pp. 123–152.
- [3] P.T.C. Harrison, Fluoride in water: a UK perspective, *J. Fluorine Chem.*, 126 (2005) 1448–1456.
- [4] S.S. Tripathy, J.-L. Bersillon, K. Gopal, Removal of fluoride from drinking water by adsorption onto alum-impregnated activated alumina, *Sep. Purif. Technol.*, 50 (2006) 310–317.
- [5] T. Nur, P. Loganathan, T.C. Nguyen, S. Vigneswaran, G. Singh, J. Kandasamy, Batch and column adsorption and desorption of fluoride using hydrous ferric oxide: solution chemistry and modeling, *Chem. Eng. J.*, 247 (2014) 93–102.
- [6] X.Z. Xiong, J.L. Liu, W.H. He, T. Xia, P. He, X.M. Chen, K.D. Yang, A.G. Wang, Dose–effect relationship between drinking water fluoride levels and damage to liver and kidney functions in children, *Environ. Res.*, 103 (2007) 112–116.
- [7] J.L. Davila-Rodriguez, V.A. Escobar-Barrios, J.R. Rangel-Mendez, Removal of fluoride from drinking water by a chitin-based biocomposite in fixed-bed columns, *J. Fluorine Chem.*, 140 (2012) 99–103.
- [8] V.K. Gupta, I. Ali, V.K. Saini, Defluoridation of wastewaters using waste carbon slurry, *Water Res.*, 41 (2007) 3307–3316.
- [9] V. Khatibikamal, A. Torabian, F. Janpoor, G. Hoshyaripour, Fluoride removal from industrial wastewater using electrocoagulation and its adsorption kinetics, *J. Hazard. Mater.*, 179 (2010) 276–280.
- [10] A. Toyoda, T. Taira, A new method for treating fluorine wastewater to reduce sludge and running costs, *IEEE Trans. Semicond. Manuf.*, 13 (2000) 305–309.
- [11] M. Agarwal, K. Rai, R. Shrivastav, S. Dass, Defluoridation of water using amended clay, *J. Cleaner Prod.*, 11 (2003) 439–444.
- [12] E.M. Nigri, A. Bhatnagar, S.D.F. Rocha, Thermal regeneration process of bone char used in the fluoride removal from aqueous solution, *J. Cleaner Prod.*, 142 (2017) 3558–357.
- [13] N.A. Medellin-Castillo, R. Leyva-Ramos, R. Ocampo-Perez, R.F. Garcia de la Cruz, A. Aragon-Piña, J.M. Martinez-Rosales, R.M. Guerrero-Coronado, L. Fuentes-Rubio, Adsorption of fluoride from water solution on bone char, *Ind. Eng. Chem. Res.*, 46 (2007) 9205–9212.
- [14] L.D. Benefield, J.F. Judkins, B.L. Weand, *Process Chemistry for Water and Wastewater Treatment*, Prentice-Hall, Englewood Cliffs, 1982.
- [15] R. Kunin, *Ion Exchange Resins*, Publishing Co., Florida, 1990.
- [16] V. Colla, T.A. Branca, F. Rosito, C. Lucca, B.P. Vivas, V.M. Delmiro, Sustainable reverse osmosis application for wastewater treatment in the steel industry, *J. Cleaner Prod.*, 130 (2016) 103–115.
- [17] P. Gwala, S. Andey, V. Mhaisalkar, P. Labhassetwar, S. Pimpalkar, C. Kshirsagar, Lab scale study on electrocoagulation defluoridation process optimization along with aluminium leaching in the process and comparison with full scale plant operation, *Water Sci. Technol.*, 63 (2011) 2788–2795.
- [18] R. Simons, Trace element removal from ash dam waters by nanofiltration and diffusion dialysis, *Desalination*, 89 (1993) 325–341.
- [19] N. Drouiche, S. Aoudj, M. Hecini, N. Ghaffour, H. Lounici, N. Mameri, Study on the treatment of photovoltaic wastewater using electrocoagulation: fluoride removal with aluminium electrodes—characteristics of products, *J. Hazard. Mater.*, 169 (2009) 65–69.
- [20] N. Mameri, A.R. Yeddou, H. Lounici, D. Belhocine, H. Grib, B. Bariou, Defluoridation of septentrional Sahara water of north Africa by electrocoagulation process using bipolar aluminium electrodes, *Water Res.*, 32 (1998) 1604–1612.
- [21] A. Guzmán, J.L. Nava, O. Coreño, I. Rodríguez, S. Gutiérrez, Arsenic and fluoride removal from groundwater by electrocoagulation using a continuous filter-press reactor, *Chemosphere*, 144 (2016) 2113–2120.
- [22] R.V. Drondina, I.V. Drako, Electrochemical technology of fluorine removal from underground and waste waters, *J. Hazard. Mater.*, 37 (1994) 91–100.

- [23] C.-L. Yang, R. Dluhy, Electrochemical generation of aluminum sorbent for fluoride adsorption, *J. Hazard. Mater.*, 94 (2002) 239–252.
- [24] F. Shen, X.M. Chen, P. Gao, G.H. Chen, Electrochemical removal of fluoride ions from industrial wastewater, *Chem. Eng. Sci.*, 58 (2003) 987–993.
- [25] M.M. Emamjomeh, M. Sivakumar, An empirical model for defluoridation by batch monopolar electrocoagulation/flotation (ECF) process, *J. Hazard. Mater.*, 131 (2006) 118–125.
- [26] J. Zhu, H.Z. Zhao, J. Ni, Fluoride distribution in electrocoagulation defluoridation process, *Sep. Purif. Technol.*, 56 (2007) 184–191.
- [27] U. Tezcan Un, A.S. Koparal, U. Bakir Ogutveren, Fluoride removal from water and wastewater with a batch cylindrical electrode using electrocoagulation, *Chem. Eng. J.*, 223 (2013) 110–115.
- [28] M.A. Sandoval, R. Fuentes, J.L. Nava, I. Rodríguez, Fluoride removal from drinking water by electrocoagulation in a continuous filter press reactor coupled to a flocculator and clarifier, *Sep. Purif. Technol.*, 134 (2014) 163–170.
- [29] M. Alimohammadi, M. Askari, M.H. Dehghani, A. Dalvand, R. Saeedi, K. Yetilmezsoy, B. Heibati, G. McKay, Elimination of natural organic matter by electrocoagulation using bipolar and monopolar arrangements of iron and aluminum electrodes, *Int. J. Environ. Sci. Technol.*, 14 (2017) 2125–2134.
- [30] U.K. Garg, C. Sharma, U.K. Garg, Electrocoagulation: promising technology for removal of fluoride from drinking water – a review, *Biol. Forum*, 8 (2016) 248–254.
- [31] B. Naraghi, M.M. Baneshi, R. Amiri, A. Dorost, H. Biglari, Removal of Reactive black 5 dye from aqueous solutions by coupled electrocoagulation and bio-adsorbent process, *Electron. Physician*, 10 (2018) 7086–7094.
- [32] M.A.G. Nasser, S.R. Rawia, N.B.F. Nader, Application of electrocoagulation on adsorption of styrene acrylate polymer from aqueous solutions, *Int. J. Sci. Res. Environ. Sci. Toxicol.*, 3 (2018) 1–11.
- [33] E. Bazrafshan, K.A. Ownagh, A.H. Mahvi, Application of electrocoagulation process using iron and aluminum electrodes for fluoride removal from aqueous environment, *E-J. Chem.*, 9 (2012) 2297–2308.
- [34] M.M. Emamjomeh, M. Sivakumar, A.S. Varyani, Analysis and the understanding of fluoride removal mechanisms by an electrocoagulation/flotation (ECF) process, *Desalination*, 275 (2011) 102–106.
- [35] A. Ezzeddine, A. Bedoui, A. Hannachi, N. Bensalah, Removal of fluoride from aluminum fluoride manufacturing wastewater by precipitation and adsorption processes, *Desal. Water Treat.*, 54 (2015) 2280–2292.
- [36] M.A. Abdel Khalek, F.I. El-Hosiny, K.A. Selim, I. Osama, Produced water treatment using a new designed electroflotation cell, *Int. J. Res. Ind. Eng.*, 6 (2017) 328–338.
- [37] P.K. Holt, G.W. Barton, M. Wark, C.A. Mitchell, A quantitative comparison between chemical dosing and electrocoagulation, *Colloids Surf., A*, 211 (2002) 233–248.
- [38] D. Ghernaout, Electrocoagulation process: a mechanistic review at the dawn of its modeling, *J. Environ. Sci. Allied Res.*, 2 (2019) 22–38.
- [39] C. Jiménez, C. Sáez, F. Martínez, P. Cañizares, M.A. Rodrigo, Electrochemical dosing of iron and aluminum in continuous processes: a key step to explain electro-coagulation processes, *Sep. Purif. Technol.*, 98 (2012) 102–108.
- [40] S. Garcia-Segura, M.M.S.G. Eiband, J.V. de Melo, C.A. Martínez-Huitle, Electrocoagulation and advanced electrocoagulation processes: a general review about the fundamentals, emerging applications and its association with other technologies, *J. Electroanal. Chem.*, 801 (2017) 267–299.
- [41] D. Ghosh, C.R. Medhi, M.K. Purkait, Treatment of fluoride containing drinking water by electrocoagulation using monopolar and bipolar electrode connections, *Chemosphere*, 73 (2008) 1393–1400.
- [42] D. Ghosh, C.R. Medhi, M.K. Purkait, Techno-economic analysis for the electrocoagulation of fluoride-contaminated drinking water, *Toxicol. Environ. Chem.*, 93 (2011) 424–437.
- [43] J.M. Babu, S. Goel, Defluoridation of drinking water in batch and continuous-flow electrocoagulation systems, *Pollut. Res.*, 32 (2013) 727–736.
- [44] APHA, Standard Methods for the Examination of Water and Wastewater, 22nd ed., American Public Health Association, Washington, D.C., USA, 2012.
- [45] M. Al-Shannag, Z. Al-Qodah, K. Bani-Melhem, M.R. Qtaishat, M. Alkasrawi, Heavy metal ions removal from metal plating wastewater using electrocoagulation: kinetic study and process performance, *Chem. Eng. J.*, 260 (2015) 749–756.
- [46] E. Nariyan, M. Sillanpää, C. Wolkersdorfer, Electrocoagulation treatment of mine water from the deepest working European metal mine – performance, isotherm and kinetic studies, *Sep. Purif. Technol.*, 177 (2017) 363–373.
- [47] J.R. Parga, V. Vazquez, H. Moreno, Thermodynamic studies of the arsenic adsorption on iron species generated by electrocoagulation, *J. Metall.*, 2009 (2009) 1–9.
- [48] J.N. Hakizimana, B. Gourich, M. Chafi, Y. Stiriba, C. Vial, P. Drogui, J. Naja, Electrocoagulation process in water treatment: a review of electrocoagulation modeling approaches, *Desalination*, 404 (2017) 1–21.
- [49] W. Den, C.-J. Wang, Removal of silica from brackish water by electrocoagulation pretreatment to prevent fouling of reverse osmosis membranes, *Sep. Purif. Technol.*, 59 (2008) 318–325.
- [50] C.-Y. Hu, S.-L. Lo, W.-H. Kuan, Simulation the kinetics of fluoride removal by electrocoagulation (EC) process using aluminum electrodes, *J. Hazard. Mater.*, 145 (2007) 180–185.
- [51] A.I. Adeogun, R.B. Balakrishnan, Kinetics, isothermal and thermodynamics studies of electrocoagulation removal of basic dye rhodamine B from aqueous solution using steel electrodes, *Appl. Water Sci.*, 7 (2017) 1711–1723.
- [52] M.H. Isa, E.H. Ezechi, Z. Ahmed, S.F. Magram, S.R.M. Kutty, Boron removal by electrocoagulation and recovery, *Water Res.*, 51 (2014) 113–123.
- [53] N.A. Medellín-Castillo, R. Leyva-Ramos, E. Padilla-Ortega, R.O. Perez, J.V. Flores-Cano, M.S. Berber-Mendoza, Adsorption capacity of bone char for removing fluoride from water solution, Role of hydroxyapatite content, adsorption mechanism and competing anions, *J. Ind. Eng. Chem.*, 20 (2014) 4014–4021.
- [54] H.M.F. Freundlich, Over the adsorption in solution, *J. Phys. Chem.*, 57 (1906) 385–471.
- [55] I. Langmuir, The constitution and fundamental properties of solids and liquids. Part I. Solids, *J. Am. Chem. Soc.*, 38 (1916) 2221–2295.
- [56] O. Redlich, D.L. Peterson, A useful adsorption isotherm, *J. Phys. Chem.*, 63 (1959) 1024–1024.
- [57] R. Sips, On the structure of a catalyst surface, *J. Chem. Phys.*, 16 (1948) 490–495.
- [58] M.I. Tempkin, V. Pyzhev, Kinetics of ammonia synthesis on promoted iron catalyst, *Acta Phys. Chim. URSS*, 12 (1940) 217–222.
- [59] CONAMA, Resolução 430, (2011). Available at: http://www.suaep.pe.gov.br/images/publicacoes/CONAMA_n.430.2011.pdf
- [60] M.M. Emamjomeh, M. Farzadkia, Fluoride removal by electrocoagulation (EC) process: aluminum chemistry and speciation, *Int. J. Adv. Sci. Eng. Technol.*, 4 (2016) 82–85.
- [61] K.Y. Foo, B.H. Hameed, Insights into the modeling of adsorption isotherm systems, *Chem. Eng. J.*, 156 (2010) 2–10.
- [62] S. Aoudj, N. Drouiche, M. Hecini, T. Ouslimane, B. Palaouane, Coagulation as a post-treatment method for the defluoridation of photovoltaic cell manufacturing wastewater, *Procedia Eng.*, 33 (2012) 111–120.
- [63] N. Drouiche, N. Ghaffour, S. Aoudj, M. Hecini, T. Ouslimane, Fluoride removal from photovoltaic wastewater by aluminum electrocoagulation and characteristics of products, *Chem. Eng. Trans.*, 17 (2009) 1651–1656.
- [64] R.L. Frost, J.T. Kloprogge, Infrared emission spectroscopic study of brucite, *Spectrochim. Acta, Part A*, 55 (1999) 2195–2205.
- [65] S. Sandhya, S. Sureshbabu, H.K. Varma, M. Komath, Nucleation kinetics of the formation of low dimensional calcium sulfate dihydrate crystals in isopropyl alcohol medium, *Cryst. Res. Technol.*, 47 (2012) 780–792.

- [66] M.P. Andersson, C.P. Hem, L.N. Schultz, J.W. Nielsen, C.S. Pedersen, K.K. Sand, D.V. Okhrimenko, A. Johnsson, S.L.S. Stipp, Infrared spectroscopy and density functional theory investigation of calcite, chalk, and coccoliths-do we observe the mineral surface, *J. Phys. Chem. A*, 118 (2014) 10720–10729.
- [67] L. Chen, G.P. Chen, X.X. Wang, H.X. Fang, C.X. Wu, T.T. Xing, Synthesis of strontium carbonate rods and hierarchical branches in the presence of two organic additives, *Cryst. Res. Technol.*, 45 (2010) 254–258.
- [68] U. Gross, S. Rüdiger, E. Kemnitz, K.W. Brzezinka, S. Mukhopadhyay, C. Bailey, A. Wander, N. Harrison, Vibrational analysis study of aluminum trifluoride phases, *J. Phys. Chem. A*, 111 (2007) 5813–5819.